Grasp Analysis and Manipulation Kinematics for Isoperimetric Truss Robots

Zachary M. Hammond, Nathan S. Usevitch, and Sean Follmer

***Abstract*— Soft isoperimetric truss robots have demonstrated an ability to grasp and manipulate objects using the members of their structure. The compliance of the members affords large contact areas with even force distribution, allowing for successful grasping even with imprecise open-loop control. In this work we present methods of analyzing and controlling isoperimetric truss robots in the context of grasping and manipulating objects. We use a direct stiffness model to characterize the structural properties of the robot and its interactions with external objects. With this approach we can estimate grasp forces and stiffnesses with limited computation compared to higher fidelity finite elements methods, which, given the many degrees-of-freedom of truss robots, are prohibitively expensive to run on-board. In conjunction with the structural model, we build upon a literature of differential kinematics for truss robots and apply it to the task of manipulating an object within the robot's workspace.**

I. Introduction

Truss robots are composed of a number of identical linear actuators that are arranged in a truss-like structure and connected by universal joints. Truss robots have inspired a wide array of research, with applications in planetary exploration [1]–[3], formation of dynamic structures [4], shoring of rubble [5], [6], burrowing [7], shape and information displays [8], [9], and as the building block of modular robotic systems [10], [11]. The coordinated deformation of the individual linear actuators enables complex shape change of the global structure. Leveraging its dynamic shape enables such a robot to adapt to the surroundings, traverse unstructured terrain, store and deploy easily, and intelligently distribute external loads among its members.

Soft isoperimetric truss robots are a recently proposed variation of truss robots that are comprised of inflated inextensible tubes that are manipulated into a truss-like structure by a collective of robotic roller modules [12]. The inflated tubes are the primary structural elements and the members of the truss structure. Each joint in the tubing is formed by a roller module that pinches the tube between cylindrical rollers, locally reducing the bending stiffness of the tube (Fig. 1a). An electric motor drives these rollers, causing the pinch point to translate. The roller modules can be connected by 3 degree-of-freedom universal joints to neighboring modules to form complex structures. Note, isoperimetric truss robots are space frames, not true truss structures.

The compliance of isoperimetric truss robots enables new modes of interaction with the outside world compared to conventional rigid truss robots. One compelling interaction is grasping and manipulating objects. The robot can change shape to engulf an object, grasp it between two members, and manipulate it in the robot's environment. Similar to soft grippers, the compliance of the structure affords large contact areas with even force distribution, allowing for successful grasping with imprecise open-loop control [13]–[18]. In order to leverage these techniques, we explore methods of analyzing and controlling isoperimetric truss robots in the context of grasping and manipulating objects.

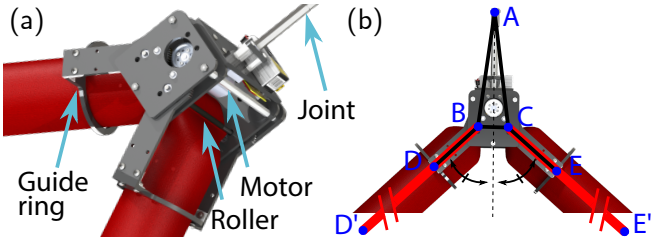

Fig. 1. (a) CAD model of a roller module of the isoperimetric truss robot. (b) The nodes and members used to describe each roller module and the adjacent segments of tube within the structural model.

An important precursor to an intelligent grasping controller is the analysis of the forces imparted on an object by the robot. Because the isoperimetric truss robot uses its own structure as a gripper, the structural behavior of the robot is highly intertwined with the grasping statics. In this work, we present a direct stiffness model of the isoperimetric truss robot and apply it in the context of grasping. We develop this model with the eventual goal of using it within a grasp optimization wherein properties of the grasp may be specified. Given the computational burden of searching the high-dimensional state-space of truss robots, we prefer models that can be computed quickly even if they only provide approximations of the grasp statics. This approach is distinct from higher fidelity finite element methods for inflatable structures, which are necessary for highly flexible and stretchable robots [19], [20]. However, due to the flexible and inextensible membrane structure, the tubes in the isoperimetric robot demonstrate an approximately linear force-displacement behavior at small displacements [12]. Therefore, we propose using a limited set of elements within our direct stiffness model.

In conjunction with grasping objects, we also want the robot to manipulate the objects within its environment. The differential kinematics describing the relationship between actuator inputs and robot shape have been described for linear actuator truss robots in [21] and applied to locomotion across flat terrain and in the presence of obstacles [22]–[25].

The authors are with the Dept. of Mechanical Engineering, Stanford University, Stanford, CA 94304, USA zhammond@stanford.edu
This work is supported in part by the National Science Foundation Award # 1925030.

Here, we build on this work in differential kinematics and apply it to the task of manipulating a grasped object. The result is a set of actuator inputs that produces a specified instantaneous motion of the grasped object. Integrated within an online controller, this kinematic solution enables the robot to follow arbitrary trajectories.

This paper is organized as follows. We describe our grasp analysis model in Section II and evaluate it in Section III. We then shift to manipulation kinematics in Section IV. Finally, we summarize the results and future directions.

II. Grasp Modeling

A. Structural Model

We use a direct stiffness model to describe the bulk mechanical properties of the isoperimetric truss robot [26]–[28]. While this can only be expected to give us approximations of structural behavior, the low computational demands of this approach are attractive for use in online optimizations. The robot is represented as a set of m members interconnected at n nodes. Each member of the structure has a linearized stiffness matrix which maps member-end deflections to member-end forces. Each member-end is either pinned (only forces are transmitted) or fixed (forces and moments are transmitted) to one node. The individual member stiffness matrices and node deflections can be aggregated together, leading to the expression:

$$F = S(x)u \tag{1}$$

where F is a vector of the external forces and moments, $S(x)$ is the aggregated stiffness matrix, and u is a vector of node displacements. Below, we describe how we identify the members and nodes of the robot model and express the member stiffness matrices in more detail. Note, in this work we only consider the 2D case for simplicity.

The isoperimetric truss robot is comprised of roller modules and inflated tubes. Each module pinches the tube at two points separated by a distance to prevent the tube from colliding with itself [12]. The module has two guide rings, which physically enforce a kinematic constraint. The guide rings are mechanically coupled such that the angle between them is bisected by the axis of the connection rod. At the end of this connection rod, the module can connect to other modules through a universal joint. The modules can be described by a set of nodes and members as shown in Fig. 1b. Node A is point where modules connect to each other. Nodes B and C are placed where the tube is pinched. Nodes D and E are placed where the tube passes through the guide rings. Nodes D' and E' belong to neighboring modules not shown. The members that constitute the module are shown in black in Fig. 1b. Roller module members BC and DE are pinned at both ends. Member BC is fixed at both ends. Member AB and AC are pinned at A and fixed at B and C, respectively.

The members comprising the segments of tube adjacent to the roller module are shown in red in Fig. 1b. Tube members BD and CE are pinned at B and C, respectively, modeling the low stiffness joint created by the pinch point. These tube members are fixed at D and E, which describes the lack of a joint at that location. However, by including these nodes, the module can exert forces on the tube at these points. Members DD' and EE' are the long segments of tube that connect to neighboring roller modules. Note, the module rollers are non-backdrivable, so we can analyze the structure quasi-statically without incorporating the stiffness characteristics of the motor and transmission.

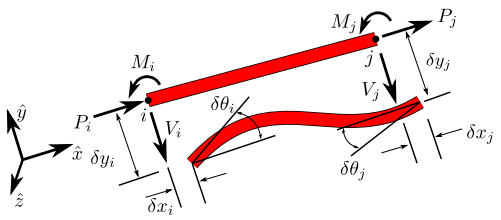

Fig. 2. The modes the members of the structure can deflect in and the loads these deflections produce.

In our model, each member in the structure can deflect in ways depicted in Fig. 2. Each member-end can deflect in the axial direction (δx), the transverse direction (δy), and rotate in the plane ($\delta\theta$). These deflections result in member loads P, V, and M, respectively. The force-displacement equation for a member can be expressed as

$$\begin{bmatrix} P_i \\ V_i \\ M_i \\ P_j \\ V_j \\ M_j \end{bmatrix} = \begin{bmatrix} \frac{\delta P}{\delta x} & 0 & 0 & \frac{-\delta P}{\delta x} & 0 & 0 \\ 0 & \frac{\delta V}{\delta y} & \frac{\delta V}{\delta \theta} & 0 & \frac{-\delta V}{\delta y} & \frac{\delta V}{\delta \theta} \\ 0 & \frac{\delta M}{\delta y} & \frac{\delta M_i}{\delta \theta_i} & 0 & \frac{-\delta M}{\delta y} & \frac{\delta M_i}{\delta \theta_j} \\ \frac{-\delta P}{\delta x} & 0 & 0 & \frac{\delta P}{\delta x} & 0 & 0 \\ 0 & \frac{-\delta V}{\delta y} & \frac{-\delta V}{\delta \theta} & 0 & \frac{\delta V}{\delta y} & \frac{-\delta V}{\delta \theta} \\ 0 & \frac{\delta M}{\delta y} & \frac{\delta M_j}{\delta \theta_i} & 0 & \frac{-\delta M}{\delta y} & \frac{\delta M_j}{\delta \theta_j} \end{bmatrix} \begin{bmatrix} \delta x_i \\ \delta y_i \\ \delta \theta_i \\ \delta x_j \\ \delta y_j \\ \delta \theta_j \end{bmatrix} \tag{2}$$

The rigid components of the roller modules are constructed of isotropic materials and can be described simply as Euler beams [27]. The nominal length of these components does not change as the robot changes configuration. The stiffness of the inflated tubes (red members BD, CE, DD' and EE' in Fig. 1), however, cannot be described by Euler beam equations. In this work we measured these stiffness values empirically and fit simple models to them. This is described in more detail in Section III. Describing the stiffness of the tubes like Hookean springs with linear force-displacement behavior is a significant simplification of reality and we should expect to see significant error at large displacements.

As the structure deforms, the members BD and CE rotate such that the angle between them is bisected by the line between node A and the midpoint of BC. This imposes a constraint for each roller module which we express as

$$\text{atan2}\left(\|v_1 \times v_2\|, v_1^T \cdot v_2\right) = \text{atan2}\left(\|v_1 \times v_3\|, v_1^T \cdot v_3\right) \tag{3}$$

where v_1 is a vector pointing from A to the midpoint of BC and v_2 and v_3 are vectors aligned with members BC and DE, respectively. We take the derivative of the constraint in (3) with respect to x and insert the result into the matrix $A(x)$. We combine these constraint equations together with the

force-displacement equations to result in our final description of the system.

$$\begin{bmatrix} F \\ 0 \end{bmatrix} = \begin{bmatrix} S(x) \\ A(x) \end{bmatrix} u = S_T(x)u \tag{4}$$

Solving the above equation for u requires the inverse of S_T. If $S_T \in \mathbb{R}^{lxl}$, the computational complexity of the inverse is $\mathcal{O}(l^3)$ with the Gauss-Jordan elimination method. Therefore, using a minimal set of nodes to describe the structure, as we have done, can have a large impact on computation time.

B. Grasp Analysis

If an object interferes with the tube as shown in Fig. 3, we would like to estimate the forces exerted on the object and the size of the contact region. In this work, we consider cylindrical objects. The first step is to create a number of new nodes in the vicinity of the object that may be in contact, breaking the single member into a number of smaller segments. These nodes are fixed to the member-ends that connect to them. When the member deflects, a portion of these nodes will be in contact with the object. The gap between any node, i, and the closest point on the surface of the object must be nonnegative (Fig. 3c). The gap, g_{ni}, is defined as

$$g_{ni} = (x_i - x_{ci})^T \hat{e}_{ni} \geq 0 \tag{5}$$

where x_i is the position of the ith node, x_{ci} is the nearest point on the surface of the object, and $\hat{e}_{ni}$ is a unit vector normal to the object surface at x_{ci}. If a node is in contact with the object, then $g_{ni} = 0$ and there could be a contact force, F_c, acting at that node (Fig. 3c)

$$F_{ci}^T \hat{e}_{ni} \geq 0 \text{ if } g_{ni} = 0 \tag{6}$$

Although surface friction is an important aspect of force closure in grasping, we ignore surface friction effects in the computation of the normal contact forces. This assumption is valid because, in most cases, the object is grasped without a tangential relative velocity with respect to the grasping members. Therefore,

$$F_{ci}^T \hat{e}_{ti} = 0 \tag{7}$$

where $\hat{e}_{ti}$ is a unit vector tangent to the object surface at x_{ci}.

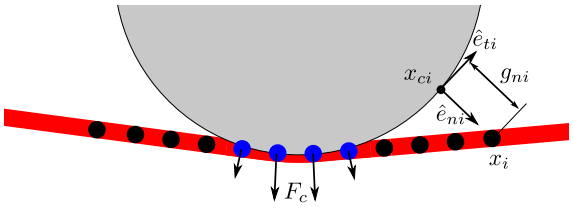

Fig. 3. An object (grey) in interference with a member (red). A number of nodes (black and blue) are added to the member in the vicinity of the object. Nodes in contact with the object (blue) exert a normal force. Nodes not in contact (black) have a positive gap size to the nearest point on the object.

Our task is to find a set of contact forces, F_c, which act on the contact candidates subject to the constraints above. Formally,

$$\begin{aligned} &\text{find} \quad F_c \\ &\text{subject to} \\ &\quad g_{ni} \geq 0 \qquad\qquad F_{ci}^T \hat{e}_{ti} = 0 \\ &\quad F_{ci}^T \hat{e}_{ni} \geq 0 \qquad\qquad F_c = Su \\ &\quad F_{ci}^T \hat{e}_{ni} g_{ni} = 0 \qquad\qquad x = x_0 + u \end{aligned} \tag{8}$$

This problem can be solved in a number of ways. Here we employ a discrete dynamic equation of F_c that converges towards a solution that satisfies all of the constraint equations. The dynamic equation is

$$\begin{aligned} F_{ci}^{p+1} = F_{ci}^p + K_1 ReLU(-g_{ni})\hat{e}_{ni} \\ - K_2 F_{ci}^T \hat{e}_{ti} \hat{e}_{ti} - K_3 ReLU(g_{ni}) F_{ci}^p \end{aligned} \tag{9}$$

The first term increases the force at a node if it is inside the object, the second term drives tangential forces to zero, and the third term drives node forces to zero if the node is not in contact with the object. These dynamics are run iteratively until the constraints of (8) are satisfied to within a specified tolerance. Given the linearity of the model, this approach converges quickly, however, the gains K_1, K_2, and K_3 must be tuned manually. The result is identification of the nodes that are in contact with the object and the normal forces acting on the object at those nodes.

Having calculated the normal contact forces in (8), we now check if they satisfy force closure. In most cases the resultant force will push the object away from the robot. Therefore, we check if there is a set of contact friction forces, F_f, that can balance the resultant force and any externally applied wrench while respecting friction limits [29]. This problem can be stated as an inequality constrained least squares optimization

$$\begin{aligned} \min_{F_f} \quad & \|DF_f - R\|_2^2 \\ \text{subject to} \quad & -\mu F_{ci} \leq F_{fi} \leq \mu F_{ci} \quad \forall\ i \end{aligned} \tag{10}$$

where D maps friction forces to wrenches on the object, R is the resultant wrench applied on the object by the normal contact forces and any externally applied wrench, and μ is the coefficient of friction. If the residual of this optimization is zero, then there is a set of friction forces that satisfy force closure.

III. Experiments and Results of Grasp Modeling

A. Inflated Tube Stiffness

A number of experiments were performed on inflated tubes to determine the stiffness relationships in (2). In each of these experiments, a tube of diameter 10.2 cm was deformed by one of the deflection modes depicted in Fig. 2 and the corresponding load was measured. On the robot, the ends of each tube segment are tapered due to the way the rollers pinch the tube. This geometry has a dramatic effect on the axial stiffness of the beam; therefore, the axial stiffness was measured when the tube was pinched between two roller modules. For the other tests, the tube was supported by guide rings on either side, mimicking the guide rings on the

TABLE I

INFLATED TUBE STIFFNESS

Model	C	b	R^2
$\frac{\delta P}{\delta x} = CP + b$	$9.64x10^{-2}$	$4.85x10^{3}$	0.98
$\frac{\delta V}{\delta y} = \frac{CP}{L} + b$	$1.24x10^{-2}$	-55.1	0.96
$\frac{\delta V}{\delta \theta} = \frac{CP}{L} + b$	$3.96x10^{-4}$	17.9	0.94
$\frac{\delta M}{\delta y} = \frac{CP}{L} + b$	$2.80x10^{-4}$	16.9	0.92
$\frac{\delta M_i}{\delta \theta_i} = C\sqrt{P} + b$	0.149	3.76	0.96
$\frac{\delta M_i}{\delta \theta_j} = \frac{CP}{L} + b$	$5.10x10^{-4}$	9.02	0.89

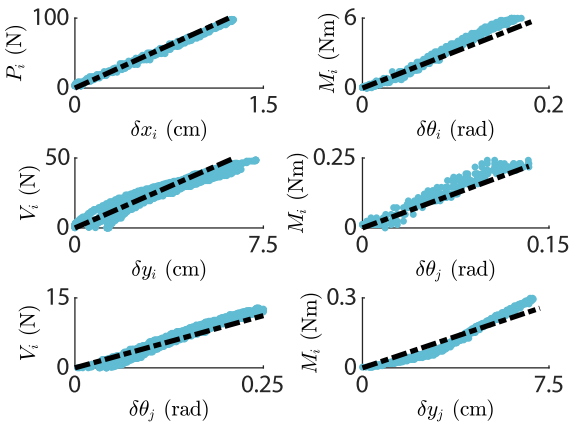

Fig. 4. Example force-displacement relationships for inflated tubes under various deflection modes. Experimental data is shown as blue dots. Linear model predictions shown in black, dashed lines.

roller modules. In tests where a member-end is translated, the member-end was secured to a freely-moving carriage on a linear track with a linear encoder to measure deflection. In tests where a member-end was rotated, the member-end was secured to a platform that rotated along with the linear travel of a carriage on the linear track. Member-end loads were measured by a Mark-10 force sensor. Each experiment was conducted over a range of three internal pressures (17.2, 34.5, and 51.7 kPa) and three undeflected member lengths (25.4, 50.8, and 76.2 cm). All permutations were repeated 5 times. A simple model was fit to the experimental data relating the member stiffness to internal pressure and member length. These models are shown in Table I. Example force-displacement curves are shown in Fig. 4.

B. Structural Stiffness

To validate the direct stiffness method for structures, we measured the force-displacement relationship of a triangular isoperimetric truss robot in three different configurations. A schematic of this robot is shown in the inset in Fig. 5. The roller module at the top of the triangle was free to move along a track in the vertical direction (y in Fig. 5). The two base modules were pinned at one of their kinematic nodes and positioned symmetrically about the linear track. A Mark-10 force sensor was pushed into the roller module along the linear track until the tubes buckle and the test was concluded.

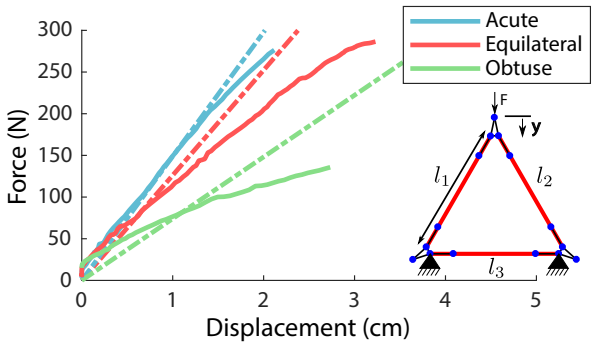

Fig. 5. Force-displacement behavior of a single triangle in three different configurations. The three configurations are obtuse triangle (edge lengths of l_1 = l_2 = 89 cm and l_3 = 128 cm), equilateral triangle (edge lengths of 102 cm), and acute triangle (edge lengths of l_1 = l_2 = 121 cm, and l_3 = 64 cm). Experimental data is shown in colored, solid lines. Model predictions are shown in black, dashed lines.

The tube diameter was 10.2 cm and the internal pressure was 34.5 kPa. The results are presented in Fig. 5. The relative relationship between the three configurations follows a similar trend to the experimental results. By repeating this test in different configurations, we show that the structural stiffness is dependent on the configuration.

C. Grasp Analysis

To validate the grasp force estimation, we conducted experiments wherein cylinders of varying diameters, d (2.54, 10.2, and 20.3 cm), were pressed into a tube at various positions along the length of the tube (Fig. 6 inset). The tube had a diameter of 10.2 cm, a length of 76.2 cm, and an internal pressure of 34.5 kPa. The objects were fixed to a Mark-10 force sensor that moved along the linear track. The linear track was positioned perpendicular to the inflated beam, and the Mark-10 measured the forces exerted along the track's direction. We use the measured force and displacement to calculate stiffness values for each trial. Averaged stiffness measurements are shown in Fig. 6 along with model predictions. In the model, we used object diameters of 12.7 cm, 20.3 cm, and 30.5 cm to account for the tube diameter. The model does a good job of estimating stiffness when d is small. However, the model is not sensitive to changes in d. This is because the model does not account for volume and pressure change of the inflated tube. Larger objects will have larger contact areas with the tube which results in a larger volume change within the tube. This volume change drives up the internal pressure and results in more force applied to the object for larger diameter objects.

We apply our grasp analysis model in simulation to a nine-member isoperimetric truss robot. Fig. 7 shows the robot in different configurations grasping an object of constant size and position. For each configuration, we can compute contact forces, contact regions, grasp stiffness, and structural deformation. The magnified view of one of the configurations in Fig. 7 visualizes the contact region, forces, and structural deflection. Grasp stiffness is calculated by displacing the object and all contact points by a specified amount and

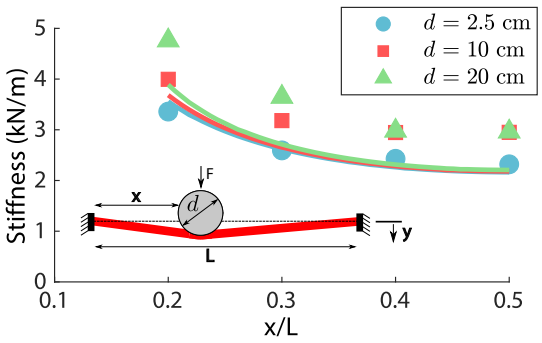

Fig. 6. Interference stiffness for tube and cylinder interaction. Experiments are shown with symbols and model predictions are shown in solid lines.

direction and then computing the resultant reaction forces at the externally constrained nodes. Each grasp configuration has a unique grasp stiffness, demonstrating that the grasp stiffness can be tuned independently of the object position.

IV. Manipulation Kinematics

Once the robot has grasped an object, it will then need to move that object around the local environment. In this section, we will describe the kinematics necessary to control the pose of a grasped object within the workspace of the isoperimetric truss robot. Here, we make the assumptions that the deformation of the structure is negligible, that the objects are of cylindrical shape, and that the two grasping members connect to the same roller module. These assumptions will be relaxed in future work. Because of the neglect of structural deformation, we can use a different set of nodes to define the configuration of the roller modules. In Fig. 8 we can see that nodes A, B, and C are the same as in Fig. 1, and nodes D and E have been removed. Nodes B' and C' correspond to nodes on neighboring roller modules. Note, the bisection constraints in (3) are now formed with B' and C' in the place of D and E.

To determine the actuation input required to affect a desired motion of the grasped object, we solve an optimization problem over the node velocities subject to constraints defined by the robot's construction and the task of manipulating a grasped object. The approach builds off work finding node velocities to move the center of mass of truss robots [21], [22]. The optimization problem can be stated as

$$\begin{aligned} \min_{\dot{x}} \quad & J(\dot{x}) \\ \text{subject to} \quad & A_{eq}\dot{x} = b_{eq} \end{aligned} \tag{11}$$

where J can be an arbitrary cost function. Here, we use $J(\dot{x}) = \dot{x}^T R_{\text{tube}}^T R_{\text{tube}} \dot{x}$ which minimizes member length change at each time step. The equality constraint, $A_{eq}\dot{x} = b_{eq}$, describes the kinematic constraints of the robot and the grasped object. In the following sections we will describe these constraints in detail.

A. Robot Kinematic Constraints

To begin, we will briefly summarize the isoperimetric robot kinematics as described in [12]. These kinematics are modified to apply to the 2D case. The forward kinematics describing the relationship between member length change, $\dot{L}$, to the motion of the nodes, $\dot{x}$, can be expressed as

$$\dot{x} = \begin{bmatrix} R_{\text{tube}}(x) \\ R_{\text{module}}(x) \\ R_{\text{bisect}}(x) \\ G \end{bmatrix}^{-1} \begin{bmatrix} \dot{L} \\ 0 \end{bmatrix} \tag{12}$$

where R_{tube} is a scaled version the rigidity matrix [30], R_{module} represents the constraints that members AB, AC, and BC are constant length, R_{bisect} represents the bisection constraints similar to those in (3), and G represents constraints to the outside world like which nodes are in contact with the ground.

Optimizing over node velocities, $\dot{x}$, requires the expression of the constraint that the tube has a constant total length in terms of node velocities. This can be written as

$$1^T \dot{L} = 1^T R_{\text{tube}}(x)\dot{x} = 0 \tag{13}$$

B. Manipulation Kinematic Constraints

The first manipulation constraint is to ensure that the robot maintains the grasp. Therefore, we add a constraint that the angle between the two grasping members remains constant. This ensures these members stay in contact with the object.

$$\text{constant} = \text{atan2}\left(\|v_1 \times v_2\|, v_1^T \cdot v_2\right) \tag{14}$$

where $v_1 = (x_{B'} - x_B)$ and $v_2 = (x_{C'} - x_C)$.

To set a constraint on the desired velocity of the object's center, we must be able to describe the velocity of this point in terms of node velocities. To do this, we establish a reference frame within which the object is stationary. This reference frame, depicted in Fig. 8, has x_B as its origin and is defined by unit vectors $\hat{e}_x$, which points to $x_{B'}$ from x_B, and $\hat{e}_y$, which is perpendicular to $\hat{e}_x$ and $\hat{z}$. We define the position of the object within this local reference frame x_{obj}. We can now relate the desired velocity of the object in the global frame in terms of node velocities as

$$\dot{x}_{des} = \frac{d}{dt}(x_B + x_{obj}) \tag{15}$$

The angular velocity of the object has two components. The first component is equivalent to the angular velocity of the local reference frame, ω_{frame}. This angular velocity can be expressed as

$$\omega_{frame} = \frac{d}{dt}\left(\text{atan2}\left((x_{B'} - x_B)\cdot\hat{y}, (x_{B'} - x_B)\cdot\hat{x}\right)\right) \tag{16}$$

It is also possible to rotate the object with respect to this local reference frame by leveraging the fact that the members are composed of continuous tubes that move relative to the roller modules like a belt through pulleys. The object rolls on the tube as it passes through the roller module, which can enable to robot to perform in-hand manipulation [12]. This angular velocity is expressed as

$$\omega_{roll} = \frac{2\dot{\phi}_i}{d} \tag{17}$$

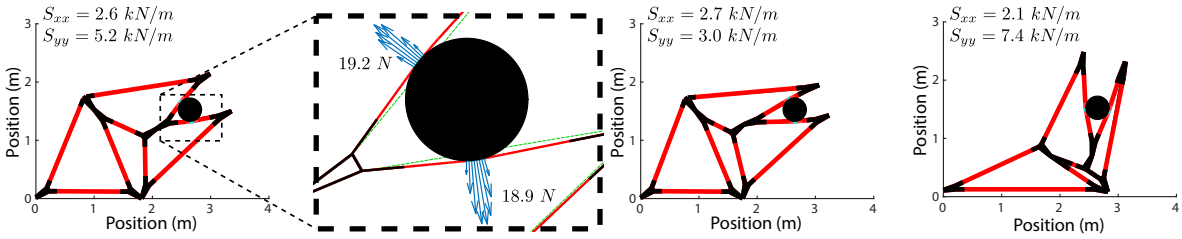

Fig. 7. Three different configuration the robot could attain to grasp an object of constant d and position. For each configuration, we can compute contact forces, contact regions, grasp stiffness, and structural deformation. The magnified view of the configuration on the left shows total force and the length of the contact region. The dashed green lines represents the robot members before the object deforms the robot.

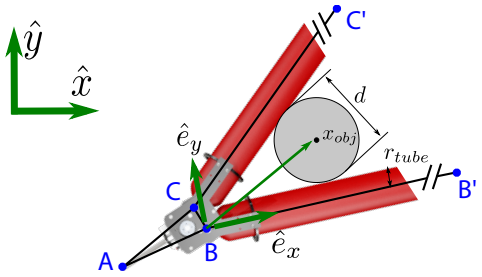

Fig. 8. The nodes (blue) and members (black) used to describe the robot kinematics and the parameters that describe the motion of the grasped object.

where $\dot{\phi}_i$ is the velocity of the nearby roller module (Fig. 8). The final constraint for the desired angular velocity can be written as

$$\omega_{des} = \omega_{frame} + \omega_{roll} \tag{18}$$

We take the derivative of (14) with respect to time and put the result, along with the results from (15) and (18), into the matrix $M(x)$ and vector b such that

$$M(x)\dot{x} = b = \begin{bmatrix} \dot{x}_{des} & \omega_{des} & 0 \end{bmatrix}^T \tag{19}$$

We can now express the optimization equality constraint as

$$A_{eq}\dot{x} = \begin{bmatrix} 1^T R_{\text{tube}}(x) \\ R_{\text{module}}(x) \\ R_{\text{bisect}}(x) \\ G \\ M \end{bmatrix} \dot{x} = \begin{bmatrix} 0 \\ b \end{bmatrix} = b_{eq} \tag{20}$$

C. Kinematics Demonstration

We demonstrate the manipulation kinematics in Fig. 9 in which a nine-member isoperimetric truss robot moves an object around its environment in simulation. The object starts in the position shown in Fig. 9a with an orientation indicated with a green arrow. The object is first translated vertically as seen in Fig. 9b. Fig. 9c shows the object's pose after a pure rotation. The path of the object during this translation is shown in blue. Fig. 9d shows the object again after it moved in a circular arc while the orientation remained normal to the curve. This simulation demonstrates that the robot is capable of performing useful tasks with a grasped object. For example, the robot can hold and reposition a workpiece during a human-robot collaborative assembly task.

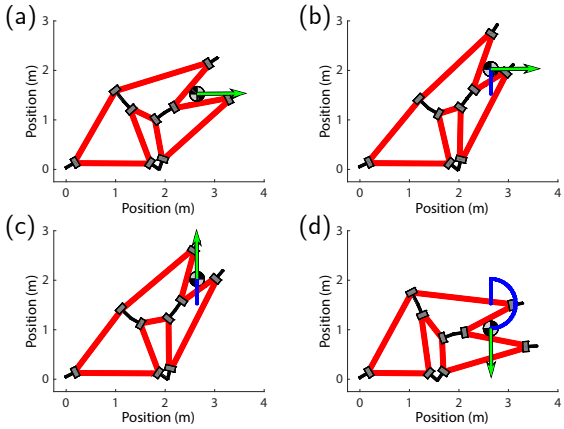

Fig. 9. A simulated isoperimetric robot moves a grasped object. The object's orientation is shown with a green arrow. The path of the object's center is shown in blue. (a) The starting configuration. (b) The object is translated vertically. (c) The object is rotated in place. (d) The object moved in a circular arc while the orientation remains normal to this curve.

V. Conclusion

Soft truss robots can leverage their compliance to grasp objects with large contact areas and even force distribution. In this paper, we have presented methods for analyzing and controlling soft isoperimetric truss robots in the context of grasping and manipulation. We developed a direct stiffness model of a soft isoperimetric truss robot using empirically determined stiffness properties of its primary structural element and compared the approach against force-displacement data taken from a simple robot. We applied this model in the context of grasp analysis and validate the model against empirical force-displacement data. In conjunction with this structural and grasp analysis, we describe the differential kinematics for truss robots manipulating a grasped object. In future work, these methods will be used within a grasp optimization that will find feasible robot grasping configurations that meet specified behavior requirements. We will investigate improvements to the model like replacing our linearized stiffness with a piecewise-linearized stiffness or other models with limited computational requirements like the discrete elastic rods method [31]. Alternatively, the model could be used in a two-tiered approach, wherein, the low-fidelity model can quickly search the configuration space to find an approximate optimum which is used to initialize a second stage optimization using a high-fidelity model.

REFERENCES

[1] G. J. Hamlin and A. C. Sanderson, "Tetrobot modular robotics: Prototype and experiments," in *Intelligent Robots and Systems' 96, IROS 96, Proceedings of the 1996 IEEE/RSJ International Conference on*, vol. 2. IEEE, 1996, pp. 390–395.

[2] P. C. Hughes, W. G. Sincarsin, and K. A. Carroll, "Trussarm—a variable-geometry-truss manipulator," *Journal of Intelligent Material Systems and Structures*, vol. 2, no. 2, pp. 148–160, 1991.

[3] S. Curtis, M. Brandt, G. Bowers, G. Brown, C. Cheung, C. Cooperider, M. Desch, N. Desch, J. Dorband, K. Gregory *et al.*, "Tetrahedral robotics for space exploration," *IEEE Aerospace and Electronic Systems Magazine*, vol. 22, no. 6, pp. 22–30, 2007.

[4] R. Kovacs, A. Ion, P. Lopes, T. Oesterreich, J. Filter, P. Otto, T. Arndt, N. Ring, M. Witte, A. Synytsia *et al.*, "Trussformer: 3d printing large kinetic structures," in *The 31st Annual ACM Symposium on User Interface Software and Technology*. ACM, 2018, pp. 113–125.

[5] A. Spinos, D. Carroll, T. Kientz, and M. Yim, "Variable topology truss: Design and analysis," in *2017 IEEE/RSJ International Conference on Intelligent Robots and Systems (IROS)*. IEEE, 2017, pp. 2717–2722.

[6] A. Spinos and M. Yim, "Towards a variable topology truss for shoring," in *2017 14th International Conference on Ubiquitous Robots and Ambient Intelligence (URAI)*. IEEE, 2017, pp. 244–249.

[7] J. C. Zagal, C. Armstrong, and S. Li, "Deformable octahedron burrowing robot," in *Artificial Life Conference Proceedings 12*. MIT Press, 2012, pp. 431–438.

[8] M. Pieber, R. Neurauter, and J. Gerstmayr, "An adaptive robot for building in-plane programmable structures," in *2018 IEEE/RSJ International Conference on Intelligent Robots and Systems (IROS)*. IEEE, 2018, pp. 1–9.

[9] Z. M. Hammond, N. S. Usevitch, E. W. Hawkes, and S. Follmer, "Pneumatic reel actuator: Design, modeling, and implementation," in *Robotics and Automation (ICRA), 2017 IEEE International Conference on*. IEEE, 2017, pp. 626–633.

[10] A. Lyder, R. F. M. Garcia, and K. Stoy, "Mechanical design of odin, an extendable heterogeneous deformable modular robot," in *Intelligent Robots and Systems, 2008. IROS 2008. IEEE/RSJ International Conference on*. Ieee, 2008, pp. 883–888.

[11] C.-H. Yu, K. Haller, D. Ingber, and R. Nagpal, "Morpho: A self-deformable modular robot inspired by cellular structure," in *2008 IEEE/RSJ International Conference on Intelligent Robots and Systems*. IEEE, 2008, pp. 3571–3578.

[12] N. S. Usevitch, Z. M. Hammond, M. Schwager, A. M. Okamura, E. W. Hawkes, and S. Follmer, "An untethered isoperimetric soft robot," *Science Robotics*, vol. 5, no. 40, 2020.

[13] E. Brown, N. Rodenberg, J. Amend, A. Mozeika, E. Steltz, M. R. Zakin, H. Lipson, and H. M. Jaeger, "Universal robotic gripper based on the jamming of granular material," *Proceedings of the National Academy of Sciences*, vol. 107, no. 44, pp. 18 809–18 814, 2010.

[14] J. Shintake, S. Rosset, B. Schubert, D. Floreano, and H. Shea, "Versatile soft grippers with intrinsic electroadhesion based on multifunctional polymer actuators," *Advanced Materials*, vol. 28, no. 2, pp. 231–238, 2016.

[15] P. Glick, S. A. Suresh, D. Ruffatto, M. Cutkosky, M. T. Tolley, and A. Parness, "A soft robotic gripper with gecko-inspired adhesive," *IEEE Robotics and Automation Letters*, vol. 3, no. 2, pp. 903–910, 2018.

[16] R. Deimel and O. Brock, "A novel type of compliant and underactuated robotic hand for dexterous grasping," *The International Journal of Robotics Research*, vol. 35, no. 1-3, pp. 161–185, 2016.

[17] J. Shintake, V. Cacucciolo, D. Floreano, and H. Shea, "Soft robotic grippers," *Advanced Materials*, vol. 30, no. 29, p. 1707035, 2018.

[18] C. Majidi, "Soft robotics: a perspective—current trends and prospects for the future," *Soft Robotics*, vol. 1, no. 1, pp. 5–11, 2014.

[19] O. Goury and C. Duriez, "Fast, generic, and reliable control and simulation of soft robots using model order reduction," *IEEE Transactions on Robotics*, vol. 34, no. 6, pp. 1565–1576, 2018.

[20] R. K. Katzschmann, M. Thieffry, O. Goury, A. Kruszewski, T.-M. Guerra, C. Duriez, and D. Rus, "Dynamically closed-loop controlled soft robotic arm using a reduced order finite element model with state observer," in *2019 2nd IEEE International Conference on Soft Robotics (RoboSoft)*. IEEE, 2019, pp. 717–724.

[21] N. Usevitch, Z. Hammond, S. Follmer, and M. Schwager, "Linear actuator robots: Differential kinematics, controllability, and algorithms for locomotion and shape morphing," in *2017 IEEE/RSJ International Conference on Intelligent Robots and Systems (IROS)*. IEEE, 2017, pp. 5361–5367.

[22] N. S. Usevitch, Z. M. Hammond, and M. Schwager, "Locomotion of linear actuator robots through kinematic planning and nonlinear optimization," *IEEE Transactions on Robotics*, 2020.

[23] S. Park, E. Park, M. Yim, J. Kim, and T. Seo, "Optimization-based nonimpact rolling locomotion of a variable geometry truss," *IEEE Robotics and Automation Letters*, vol. 4, no. 2, pp. 747–752, 2019.

[24] S. Park, J. Bae, S. Lee, M. Yim, J. Kim, and T. Seo, "Polygon-based random tree search planning for variable geometry truss robot," *IEEE Robotics and Automation Letters*, vol. 5, no. 2, pp. 813–819, 2020.

[25] C. Liu, S. Yu, and M. Yim, "A fast configuration space algorithm for variable topology truss modular robots," in *2020 International Conference on Robotics and Automation (ICRA), Paris, France*, 2020.

[26] K. Leet, C.-M. Uang, and A. M. Gilbert, *Fundamentals of structural analysis*. McGraw-Hill Higher Education, 2008.

[27] W. McGuire, R. H. Gallagher, and R. D. Ziemian, *Matrix structural analysis*, 2000.

[28] P. Wriggers, *Nonlinear finite element methods*. Springer Science & Business Media, 2008.

[29] M. T. Mason and J. K. Salisbury Jr, "Robot hands and the mechanics of manipulation," 1985.

[30] L. Asimow and B. Roth, "The rigidity of graphs," *Transactions of the American Mathematical Society*, vol. 245, pp. 279–289, 1978.

[31] M. Bergou, M. Wardetzky, S. Robinson, B. Audoly, and E. Grinspun, "Discrete elastic rods," in *ACM SIGGRAPH 2008 papers*, 2008, pp. 1–12.